

High-Speed State Estimation in Power Systems with Extreme Unobservability Using Machine Learning

Antos Cheeramban Varghese, *Student Member, IEEE*, Hritik Shah, *Student Member, IEEE*, Behrouz Azimian, *Student Member, IEEE*, Anamitra Pal, *Senior Member, IEEE*, Evangelos Farantatos, *Senior Member, IEEE*, Mahendra Patel, *Senior Member, IEEE*, and Paul Myrda, *Senior Member, IEEE*

Abstract—Fast timescale state estimation for a large power system can be challenging if the sensors producing the measurements are few in number. This is particularly true for doing *time-synchronized* state estimation for a transmission system that has minimal phasor measurement unit (PMU) coverage. This paper proposes a Deep Neural network-based State Estimator (DeNSE) to overcome this extreme unobservability problem. For systems in which the existing PMU infrastructure is not able to bring the estimation errors within acceptable limits using the DeNSE, a data-driven incremental PMU placement methodology is also introduced. The practical utility of the proposed approach is demonstrated by considering topology changes, non-Gaussian measurement noise, bad data detection and correction, and large system application.

Index Terms—Deep neural network (DNN), Phasor measurement unit (PMU), State estimation, Unobservability.

I. INTRODUCTION

Power system static state estimation is concerned with estimating the voltage magnitudes and angles of all the buses in the system [1]-[4]. Traditionally, this had been done using the supervisory control and data acquisition (SCADA) system that polled remote terminal units to get the relevant measurements. With the introduction of phasor measurement units (PMUs) into the power system, hybrid state estimation (HSE) and linear state estimation (LSE) was proposed. HSE *directly* combines SCADA and PMU data for performing state estimation [2]. However, the temporal differences in the two sets of measurements and absence of time-synchronization in the SCADA data impacts the use of HSEs for fast timescale (sub-second) applications [3]. LSE produces time-synchronized estimates of the states at high-speeds but requires complete observability of the system by PMUs for its successful execution [4]. Many real-world systems do not have the infrastructure in place to satisfy this constraint. For example, a power utility in the US Eastern Interconnection has PMUs placed on only 184 buses when its transmission system has 16,000+ buses. Moreover, the centralized nature of the classical LSE formulation limits its use for large networks due to the need of an extensive communication infrastructure [5].

Purely PMU-based multi-area state estimation and partitioned LSE have been proposed in the past for overcoming the communication limitations. A multi-level partitioning

algorithm was proposed in [6] where the system was split to create copies of the same network. State estimation was performed independently for the individual copies and then averaged to obtain the states of the whole system. However, [6] required redundant observability of the system by PMUs. A partitioned LSE using PMUs was proposed in [7] with the aim of minimizing information exchange between the partitioned regions. However, [7] required the partitioned regions to be completely observed by PMUs. *Time-synchronized* state estimation for a system that is *extremely sparsely observed by PMUs* is a challenging problem that has not been well-explored.

One way to counteract unobservability is to use pseudo-measurements obtained by interpolated observations or forecasts obtained using historical measurements. However, such an approach does not ensure quality of the estimates (see [8]). The use of machine learning (ML) for addressing the observability issues w.r.t. high-speed state estimation has been proposed in [9]-[11]. Ref. [9] proposed a Bayesian state estimator using deep neural networks (DNNs), but it was tailored for distribution systems. An ML-based state estimator for incompletely observed transmission systems was created in [10]. A state estimator with two DNNs (one for observable and the other for unobservable parts of the network) was proposed in [11]. However, [10] and [11] did not propose a systematic approach for improving the estimator's performance with addition of new sensors. To the best of the authors' knowledge, *no prior literature has analyzed time-synchronized state estimation performance as a function of PMU coverage in a transmission system with severe unobservability*. The Deep Neural network-based State Estimator (DeNSE) framework proposed in this paper addresses this issue by (a) *indirectly* combining inferences drawn from slow timescale historical SCADA data with fast timescale PMU data, and (b) determining minimal locations where *additional* PMUs must be placed to ensure satisfactory performance. Moreover, by performing state estimation using very few PMUs, the proposed approach also circumvents the need for a massive supporting communication infrastructure.

Apart from the unobservability issue, there are several other challenges that exist w.r.t. time-synchronized transmission system state estimation (TSSE). One challenge is the *scalability* of the state estimation technique to large networks [11]. The classical LSE formulation involves a matrix inversion step,

This work was supported in part by the U.S. Department of Energy under grant DE-EE0009355, the National Science Foundation under the grant ECCS-2145063, and by the Electric Power Research Institute (EPRI) under grant 10013085.

Antos Cheeramban Varghese (email: avarghef6@asu.edu), Hritik Shah (email: hshah59@asu.edu), Behrouz Azimian (email: bazimian@asu.edu), and

Anamitra Pal (email: Anamitra.Pal@asu.edu) are with the School of Electrical, Computer, and Energy Engineering of Arizona State University.

Evangelos Farantatos (email: efarantatos@epri.com), Mahendra Patel (email: mpatel@epri.com), and Paul Myrda (email: pmyrda@epri.com) are with EPRI.

Antos C. Varghese and Hritik Shah are co-first authors.

whose computational complexity is $O(n^{2.3727})$ [12]. As such, the time consumption of this implementation increases quadratically w.r.t. the number of states. Conversely, during online implementation, the forward propagation of a neural network only involves multiplication and addition operations, whose complexity ($O(n \log n)$) is much lower [13]. Another challenge is the *presence of non-Gaussian noise* in PMU measurements [14]-[17]. The LSE formulation is the solution to the maximum likelihood estimation (MLE) problem under Gaussian noise environments. This means that its performance can deteriorate in presence of non-Gaussian noise. However, a neural network-based framework, such as the DeNSE, does not have such a limitation. The third challenge is *high-speed bad data detection and correction (BDDC)* [18]. Dearth of measurements makes this challenge particularly acute for the problem being solved here. To address this challenge, a robust BDDC algorithm based on a combination of the Wald test [19] and an extreme scenario filter, is developed. The fourth challenge is *handling topology changes* and is specific to ML-based state estimators. This challenge is tackled by combining topology processor outputs with Transfer learning [20].

In summary, this paper advances the state-of-the-art for time-synchronized state estimation in transmission systems by making the following salient contributions:

1. A high-speed ML-based state estimator (DeNSE) is developed for the transmission system that overcomes the need to extensively observe the system by PMUs.
2. A novel incremental PMU placement algorithm is proposed in case the existing PMUs are not able to provide desired state estimation accuracy.
3. A robust BDDC methodology is created that ensures performance of the DeNSE under diverse conditions.
4. The ability of the DeNSE to tackle topology changes and non-Gaussian measurement noise is demonstrated.
5. The scalability of the DeNSE framework is proved by performing state estimation on a 2,000-bus test system.

II. PROPOSED FORMULATION

A. Bayesian-approach to TSSE

PMU-based LSE essentially solves some variant of the MLE problem, with the most common being the least squares (LS) formulation. However, a LS solution requires the system of equations to have full rank, which translates to the well-known constraint of complete system observability by PMUs [21], [22]. One way to circumvent this constraint is to reformulate the TSSE problem within a Bayesian framework where the states, x , and the PMU measurements, z , are treated as random variables. Then, the following minimum mean squared error (MMSE) estimator can be formulated:

$$\min_{\hat{x}(z)} \mathbb{E}(\|x - \hat{x}(z)\|^2) \Rightarrow \hat{x}^*(z) = \mathbb{E}(x|z) \quad (1)$$

Eq. (1) directly minimizes the *estimation error* without the knowledge of the physical model of the system. Note that in the classical LSE formulation, $z = Hx + e$, the *modeling error* is minimized which is embedded in the measurement function, H , that maps the states to the measurements. By avoiding the explicit need for H , the observability requirement is no longer necessary in the Bayesian framework. Furthermore, by directly minimizing the estimation error, no limitation (Gaussian/non-

Gaussian) is imposed on the characteristics of the measurement error, e . However, there are two challenges in computing the expected conditional mean of (1). First, the conditional expectation, defined by $\mathbb{E}(x|z) = \int_{-\infty}^{+\infty} xp(x|z)dx$, requires the knowledge of the joint probability density function (PDF) between x and z , denoted by $p(x, z)$. When the number of PMUs is scarce, $p(x, z)$ is unknown or impossible to specify, making direct computation of $\hat{x}^*(z)$ intractable. Second, even if the underlying joint PDF is known, finding a closed-form solution for (1) can be difficult. A DNN is used here to approximate the MMSE state estimator since a DNN has excellent approximation capabilities [23].

B. Architecture of the DNN in the DeNSE framework

The DNN used in the DeNSE framework has a feed-forward architecture comprising m inputs in the input layer and n outputs in the output layer, where m corresponds to the measurements obtained from installed PMUs and n refers to the total number of states to be estimated. Due to incomplete observability of the system by PMUs, $m \ll n$. The DNN has h hidden layers, in which the input vector entering the $(i + 1)^{th}$ layer is expressed in terms of the inputs from the i^{th} layer as:

$$c_{i+1} = W_{i+1,i} d_i + b_{i+1} \quad (2)$$

where c_{i+1} represents the input vector entering the $(i + 1)^{th}$ layer, $W_{i+1,i}$ represents the weight between the i^{th} and the $(i + 1)^{th}$ layer, d_i denotes the output of the i^{th} layer, and b_{i+1} represents the bias value in the $(i + 1)^{th}$ layer. Next, c_{i+1} is passed through an activation function, a_{i+1} , to yield d_{i+1} :

$$d_{i+1} = a_{i+1}(c_{i+1}) \quad (3)$$

This propagation continues through all the hidden layers and the resulting value is obtained at the output layer. The loss function compares the estimated output and corresponding true output. The error between them is represented by:

$$e_j = \zeta(o_j, \hat{o}_j) \quad (4)$$

where e_j denotes the error, o_j denotes the true value of the output and \hat{o}_j denotes the estimated value of the output by the DNN in the current epoch; ζ is an appropriate loss function that indicates how well the DNN has been trained. To improve the training accuracy, ζ is minimized by optimally tuning the weights and biases through a process called backpropagation. The process is repeated until the loss becomes acceptable.

C. Creation of Training Database

A unique feature of the DeNSE framework that sets it apart from other ML-based state estimators (such as [24]) is that it *does not use* the slow timescale measurements directly in the DNN training. Instead, the discrete measurements from the SCADA system are first converted into continuous functions by fitting an appropriate distribution to them. Then, Monte Carlo (MC) sampling is employed to randomly sample points from the distribution and fed as inputs to a power flow solver. The outputs of the power flow solver that correspond to voltage and current phasors measured by installed PMUs are used to train the DNN. This decoupling of the use of PMU and SCADA data for training the DNN serves two purposes: (a) the problem of temporal differences and synchronization issues are completely circumvented, and (b) any reasonable errors in the SCADA data

do not impinge on the performance of the DeNSE. However, the proposed state estimator can be impacted by the noise present in the actual PMU measurements as they are directly fed into the trained DNN during the online operation. This is investigated in detail in Section IV.C.

D. Incremental PMU Placement

The proposed DeNSE will first try to estimate all the system states using existing PMUs. However, in an actual transmission system, PMUs are placed in a *locally dense* manner; i.e., the few highest voltage buses are completely (often redundantly) observed, whereas large portions of the lower voltages are mostly unobserved. Consequently, despite extensive training, it is possible that the estimation errors of the PMU-unobservable regions remain higher than the PMU-observable regions. In conventional approaches, this problem is overcome by adding more PMUs to the system, with the objective of *maximizing system observability* with every new PMU [25]. However, since a DNN is aimed at approximating the joint PDF between its inputs (measurements) and outputs (states), such an approach will not work for the proposed state estimator. An incremental sensor placement algorithm was developed by the authors in [9] to facilitate distribution system state estimation. The algorithm exploited the high correlations that exist between the nodes since the distribution system is usually operated in a radial manner. However, such an approach will not work for *meshed* transmission systems. Therefore, a novel incremental PMU placement methodology is proposed here for the transmission system whose objective is to *minimize the estimation error* with every additional PMU.

Two observations that drive the proposed incremental PMU placement methodology are as follows: *It is difficult for the DNN to estimate the joint PDF between the measurements and the states when (a) the measurements are far away from the states, and (b) the measurements have very high variability.* The first observation is self-explanatory, but the second one is more intuitive. It refers to the fact that the DNN is essentially trying to find the relationship that governs how a change in the measurements affects the states. The measurements used in the DeNSE framework are voltage and current phasor measurements from PMUs. However, the variability in a power system comes from the fluctuations that take place in the generation and loads. Therefore, the bus power injections obtained during the creation of the training database are used to determine the locations that have the highest variability.

Taking these two observations into consideration, **Algorithm I** is created to determine the locations where new PMUs must be placed to facilitate TSSE. In **Algorithm I**, μ_{MAE} denotes the average mean absolute errors (MAEs) of every output feature, and ϵ denotes the threshold value for the same. The incremental PMU placement algorithm is run until μ_{MAE} becomes lower than ϵ . Note that after every new PMU is added in accordance with this algorithm, the DNN training and validation must be performed afresh. **Algorithm I** helps in bringing down the validation errors in the state estimates below the desired limits with minimal number of additional PMUs. This algorithm is an important contribution because to the best of the authors' knowledge no systematic approach currently exists to *improve the performance of a ML-based state estimator for the transmission system* of a power system.

Algorithm I: Incremental PMU placement for improving performance of the DeNSE

Input: Existing PMU locations, L_{init} ; Bus power injections, P ; Adjacency matrix of the system, A

Output: Final PMU locations, L

1. Set $L = L_{init}$
 2. Run the DeNSE using measurements from PMUs found in L to calculate μ_{MAE}
 3. While ($\mu_{MAE} \geq \epsilon$):
 - i. $j = \text{Length}(L)$
 - ii. Using A and L , compute d_i , the number of hops of i^{th} bus to the nearest PMU bus
 - iii. Using P , compute $\sigma_{p,i}$, the standard deviation of power injection of i^{th} bus
 - iv. Calculate the product, $Q_i = d_i \times \sigma_{p,i}$
 - v. Find the bus which has highest value of Q_i , i.e., $l = \arg \max_i Q_i$
 - vi. $L = L + \{l\}$
 - vii. Go to Step 2
 4. End While
-

III. ENHANCEMENTS TO PROPOSED FORMULATION AND ONLINE IMPLEMENTATION

A. Transfer Learning to Handle Topology Changes

A DNN trained using the formulation proposed in Section II will perform fast and accurate time-synchronized state estimation during online implementation for PMU-unobservable transmission systems as long as the topology of the system does not change. However, if the topology used for training and implementation become different, then the joint PDF between the measurements and the states will change; this can deteriorate performance of the DeNSE. A possible alternative is to train the DNN from scratch for the new topology. However, it will take a very long time to do so. Instead, we use Transfer learning to update the DNN of the DeNSE when topology changes.

Transfer learning refers to utilizing features learned from an old problem and leveraging them for a new problem to maintain learning performance and accuracy. In the context of TSSE, Transfer learning is particularly useful because when a topology change occurs, the mapping between measurements and states of only a small portion of the system gets altered. This implies that the re-learning will be localized. We employ inductive transfer learning [26], to induce knowledge transfer from the old (base) topology to the new (current) topology.

Four approaches have been proposed for implementing inductive transfer learning: feature-representation transfer, instance transfer, relational-knowledge transfer, and parameter transfer [27]. We use parameter transfer here to update the parameters of the DNN when topology changes. Two well-known parameter transfer methods are parameter-sharing and fine-tuning. Parameter-sharing assumes that the parameters are highly transferable due to which the parameters in the source domain (old topology) can be directly copied to the target domain (new topology), where they are kept "frozen". Fine-tuning assumes that the parameters in the source domain are useful, but they must be trained with limited target domain data to better adapt to the target domain [28]. Since there is no guarantee that the parameters of the DNN will be highly

transferable for different topologies, *fine-tuning* is used in this paper for performing Transfer learning.

To determine when Transfer learning via fine-tuning should be implemented, we make use of the topology processor of the transmission system. After updating the DNN, the new topology is designated as the base topology, to make it consistent with the DeNSE. The overall implementation is shown in Figure 1.

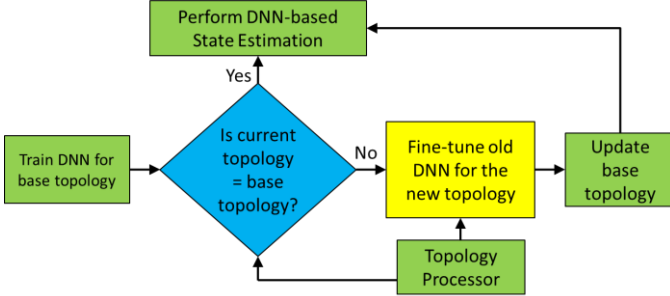


Figure 1: Implementation of Transfer learning to handle topology changes

B. Robust Bad Data Detection and Correction (BDDC)

During online implementation, streaming PMU data will be fed as inputs to the proposed DeNSE framework. However, PMU data obtained from the field often suffers from bad data in the form of data dropouts and stale data [29]. To prevent such data from impacting the performance of the DeNSE, a robust BDDC methodology must be devised as a precursor to this state estimator. The devised methodology must be compatible with the DeNSE in the sense that it must be able to operate at PMU timescales (typically 30 samples per second).

1) BDDC using Wald test

A technique to detect bad data before it can enter an ML-based state estimator was proposed in [8]. The technique relied on the Wald test [19] to flag incoming measurements as bad. To apply this test, two hypotheses must be defined first: (a) H_0 : models the measurement without bad data and has a Gaussian distribution with mean, μ_0 , and variance, σ_0^2 , both of which are learned during training. (b) H_1 : models the measurement with bad data, because of which its mean and standard deviation are very different from that of H_0 . Mathematically, the Wald test can be expressed as:

$$\left| \frac{z - \mu_0}{\sigma_0} \right| \underset{H_0}{\geq} \underset{H_1}{=} Q^{-1} \left(\frac{\alpha}{2} \right) \quad (5)$$

In (5), $Q(y) = \frac{1}{\sqrt{2\pi}} \int_y^\infty \exp\left(-\frac{u^2}{2}\right) du$, is the Gaussian tail of the PDF and α is a tunable parameter that specifies the false positive limit. Essentially, the Wald test takes advantage of the fact that DNN training is done using normalized inputs that have good quality. Hence, once the expected limits of good quality data become known during training, any testing data that lies outside that limit can be termed as bad.

The Wald test-based bad data detection method developed in [8] was found to be compatible with the proposed high-speed time-synchronized state estimator. However, [8] corrected the identified bad data by simply replacing it with its mean value from the training database. The methodology for correcting the bad data is different in this paper, as explained below.

We first note that Wald test is applied independently and simultaneously to all the m input features of a given sample of the testing dataset. Now, it is highly unlikely that all the input

features of the testing dataset sample will be bad at the same time. For a given testing dataset sample, z_{sample}^{test} , let the set of indices that correspond to features flagged as bad by the Wald test be called $ibfs$. Then, if $iafs$ denotes the set of indices corresponding to all the features of z_{sample}^{test} , the difference of these two sets gives the set of indices corresponding to the good features of z_{sample}^{test} ; let this set be denoted by $igfs$. Now, $igfs$ can be used to find that operating condition (OC) in the training database, y^{train} , which most closely resembles the OC captured by z_{sample}^{test} . Once that OC is found, its entries corresponding to $ibfs$ should replace the flagged features of z_{sample}^{test} . The overall methodology is depicted in **Algorithm II** and is performed for every sample of the testing dataset. The superiority of the proposed bad data correction methodology over the one where it is replaced with mean values is demonstrated in Section IV.D.

Algorithm II: Novel bad data correction methodology using nearest OC in training dataset

Input: $z_{sample}^{test}, y^{train}$

Output: The corrected testing dataset sample, $z_{sample_corr}^{test}$

1. Create array of indices, $iafs$, from z_{sample}^{test} , and set $z_{sample_corr}^{test} = z_{sample}^{test}$
 2. Conduct Wald test on z_{sample}^{test} and flag the indices of bad data to create $ibfs$
 3. $\{igfs\} = \{iafs\} - \{ibfs\}$
 4. $k^* = \arg \min_k \|y^{train}[k, igfs] - z_{sample}^{test}[igfs]\|$
 5. $z_{sample_corr}^{test}[ibfs] = y^{train}[k^*, ibfs]$
-

2) Differentiating between bad data and extreme scenarios

One caveat of using the Wald test to detect bad data is that it is very sensitive to the choice of α . A very small value of α may result in a bad data being treated as a good data, while a very large value may result in an extreme scenario data being treated as a bad data. This can happen because by definition extreme scenarios are those OCs which are unlikely to occur normally. In the worst-case, data corresponding to an extreme scenario will get flagged as bad data and be replaced by a normal data from the training database, which will then make the DeNSE produce an incorrect picture of the operating state of the system. We combine our knowledge of how PMUs are placed in a power system with how extreme OCs actually manifest, to design an *extreme scenario filter* that prevents this problem.

Power utilities typically place PMUs on their highest voltage buses first (i.e., *locally dense* PMU placement). As the highest voltage lines connect these buses, the PMUs placed on them will be electrically close to each other even for PMU-unobservable transmission systems. Therefore, when an extreme scenario manifests, measurements of multiple PMUs will be simultaneously impacted. Conversely, bad data occurs randomly in both space and time. This realization led us to propose the following logic for the design of the extreme scenario filter: *If one or more features of the testing data sample are simultaneously identified as bad by the Wald test for p different PMUs, each of which are within p hops of each other, then the data sample corresponds to an extreme OC and should not be treated as bad data.* This logic is implemented in the manner shown in **Algorithm III**.

Algorithm III: Extreme scenario filter implementation**Input:** Features flagged as bad by Wald test, $ibfs$ **Output:** Features passing extreme scenario filter, $ibfs_{ESF}$

1. ESF_{ini} = PMU locations corresponding to $ibfs$
2. $p = \text{Length}(ESF_{ini})$
3. $ibfs_{ESF} = ibfs$
4. ESF_p = List of subsets of ESF_{ini} with p elements
5. For ($k = 1: \text{Length}(ESF_p)$):
 - a. If (every element of $ESF_p[k]$ is within p hops of each other):
 - i. $Feat_{ESF}$ = List of all features corresponding to $ESF_p[k]$
 - ii. $\{ibfs_{ESF}\} = \{ibfs_{ESF}\} - \{Feat_{ESF}\}$
 - b. End If
6. End For
7. $p = p - 1$
8. If ($(ibfs_{ESF} \neq ibfs)$ or ($p < 2$)):
 9. End
10. Else Go to Step 3

Note that in **Algorithm III**, p indicates the severity of the extreme scenario; higher the value of p , a greater number of hops to be considered. Lastly, the extreme scenario filter is combined with the proposed BDDC methodology in the following way: whenever the filter gets activated, the results of the Wald test are suppressed (i.e., no data correction occurs), and the raw PMU measurements are fed as an input to the trained DNN of the DeNSE. The usefulness of the extreme scenario filter in making the working of DeNSE more realistic is demonstrated in Section IV.E.

C. Implementation of DeNSE

Figure 2 shows the overall framework for the proposed DeNSE. It has an offline learning phase and an online implementation phase. In the offline phase, appropriate PDFs are fitted to discrete historical data from the SCADA system using Kernel density estimation (KDE) [30]. MC sampling is done from the fitted PDFs and set as inputs to a power flow solver to generate training data for the DNN. The voltage and current phasors corresponding to actual PMU locations are used to train the DNN while all the voltage phasors (states) are set as outputs of the DNN. Once the optimized DNN parameters are found, the DNN training is set to be complete. In the online phase, streaming PMU data is fed as inputs to the trained DNN (after passing through the Wald test and a data preprocessing block), and the state estimates are obtained at its outputs.

IV. RESULTS AND DISCUSSION

A. State Estimation Results for IEEE 118-Bus System

The effectiveness of the DeNSE is first illustrated using the IEEE 118-bus system. Each bus of this system is mapped to a bus in the 2000-bus Synthetic Texas system [31] of similar mean power rating. This is done because the Texas system has one-year worth of SCADA data publicly available, and this mapping helps in obtaining realistic variations in the active and reactive powers for each bus of the 118-bus system. Next, the PDFs of the power injections are found using KDE. After picking samples independently from the PDFs, a power flow is solved to create the training, validation, and testing databases.

The training and testing of the DNN is carried out using the TensorFlow library in Python. To overcome the problem of internal covariate shift, batch normalization is employed. Dropout regularization is used to prevent DNN overfitting. Rectified linear unit (ReLU) activation function is used in the hidden layers, while a linear function is used in the output layer. The mean squared error (MSE) loss function is used to calculate the error between the predicted and the true states. During back-propagation, the Adam optimizer is used to update the weights of the DNN. Table I summarizes the optimal hyperparameters obtained of the DeNSE for the 118-bus system; hyperparameter tuning was done using WandB [32]. All simulations were performed on a computer with 256 GB RAM, Intel Xeon 6246R CPU @3.40GHz, Nvidia Quadro RTX 5000 16 GB GPU.

Initially, PMUs were assumed to be placed on only the 11 highest voltage buses of this system (namely, 8, 9, 10, 26, 30, 38, 63, 64, 65, 68, and 81). When data from these PMUs were fed into the DeNSE, the average magnitude mean absolute percentage error (MAPE) and average angle MAE were 0.1679% and 0.0120 rad, respectively. Note that under 1% total vector error (TVE) [33] Gaussian noise environments and with 32 locations where PMUs were placed, LSE gave a magnitude and angle error of 0.2709% and 0.0026 rad, respectively. This result implies that additional PMUs are needed to improve the estimation performance (particularly, for angles) of the DeNSE for the 118-bus system.

To place additional PMUs, **Algorithm I** was employed, and the LSE results were set as the threshold. With two additional locations, namely, buses 90 and 106, the DeNSE performance was comparable with LSE for angle estimates and much better for magnitude estimates. The results of the DeNSE obtained with PMUs placed at 13 buses of the 118-bus system is shown in Figure 3. Note that for obtaining the results shown in this paper, it is assumed that whenever a bus is selected for PMU placement, all the currents that come out of that bus are monitored by PMUs. Therefore, although the number of bus locations where PMUs were placed was 13, the actual number of phasor measurements were 49 (= 13 voltage phasor measurements and 36 current phasor measurements). At the same time, the number of states that were estimated was 118 voltage phasors (one per bus), which is much more than 49. Moreover, for the results depicted in Figure 3, the average magnitude MAPE was 0.1507% while average angle MAE was

Table I: Hyperparameters for DeNSE for IEEE 118-bus system

Hyperparameter	Value
Number of Hidden Layers	4
Number of Neurons per Hidden Layer	500
Activation Functions	ReLU (Hidden Layers) Linear (Output Layer)
Loss Function	Mean Squared Error
Optimizer	Adam
Batch Size	128
Learning Rate	0.0207
Number of Epochs	2,000
Early Stopping	Patience = 10
Dropout	30%
Dataset size	
Training	7,500
Validation	2,500
Testing	4,000
Total	14,000

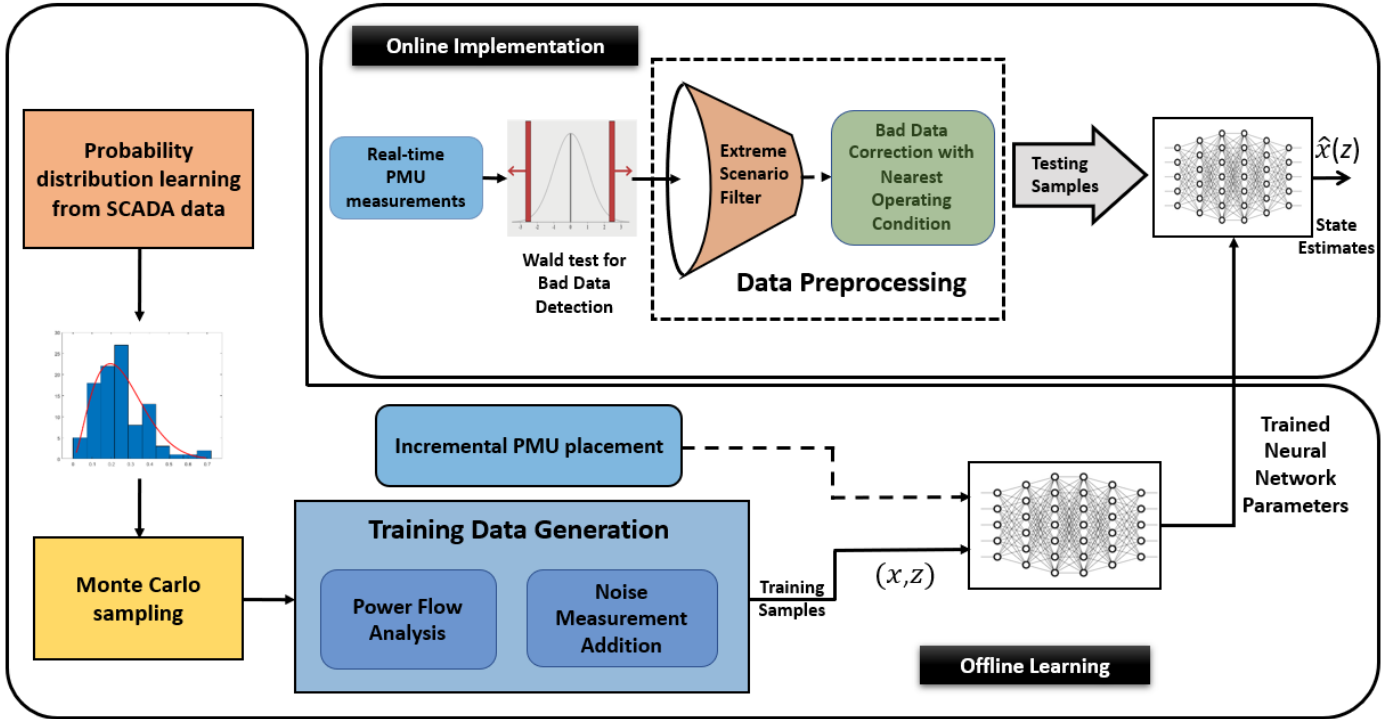


Figure 2: Proposed Bayesian framework for DeNSE. The dashed box denotes the preprocessing module, while the dotted arrows (incremental PMU placement and output of extreme scenario filter) indicate actions that are performed only when needed

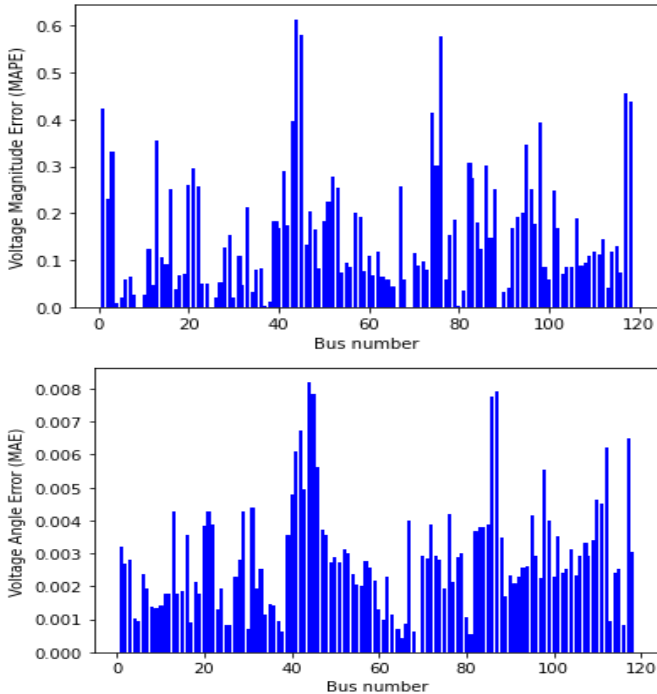


Figure 3: ML-based state estimator performance with PMUs placed at 13 buses of the IEEE 118-bus system

0.0027 rad. These results prove that high accuracy is achieved by the DeNSE even in presence of severe unobservability.

B. Impact of Topology Changes

To investigate the ability of Transfer learning in updating the DNN of DeNSE after topology changes, a set of likely topologies were identified for the 118-bus system. These topologies were created by removing one line at a time between

any two buses of the system, such that an island is not formed; 177 such topologies were identified. The training data for these likely topologies were saved in the database. When a topology change is detected by the topology processor in real-time, Transfer learning via fine-tuning is activated as described in Figure 1. The results obtained are as follows.

Let the base topology be denoted by T_1 . By opening different lines, three new topologies were created from T_1 . T_2 was created by opening the line between buses 103 and 110, neither of which have a PMU on them. T_3 was obtained when the line between buses 89 and 90 was removed; note that bus 90 has a PMU on it. T_4 was realized by opening the line between buses 26 and 30, both of which have a PMU on them. Figure 4 and Figure 5 show the changes in topology and their influence on TSSE with and without Transfer learning.

When Transfer learning is used to update the DNN, fine-tuning only takes 30 seconds of re-training time to give similar results for the new topologies as was obtained for the base topology (the heights of the grey and blue bars are similar). Note that if we had trained the DNN from scratch for every new topology, it would have taken 3 hours for every topology change, making the DeNSE inconsistent with the current state of the system for a much longer time-period. The reason why fine-tuning is so fast is because it only needs 2,000 samples and 90 epochs compared to 10,000 samples and 2,000 epochs that were needed to train the DNN from scratch (see Table I). Conversely, if the DNN trained for T_1 is used throughout, the performance of DeNSE degrades significantly (compare the heights of blue and orange bars in Figure 4 and Figure 5). It can be also observed from the two figures that the deterioration in estimation is more prominent for T_3 and T_4 . This happens because the line that was opened for creating these two topologies had PMUs placed on one and both ends of the line,

respectively. As such, there was a considerable difference in the training and testing environments for these two topologies in comparison to T_1 .

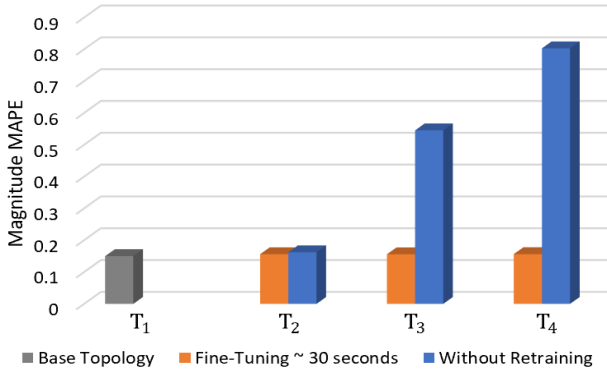


Figure 4: Efficacy of Transfer learning – average Magnitude MAPE in %

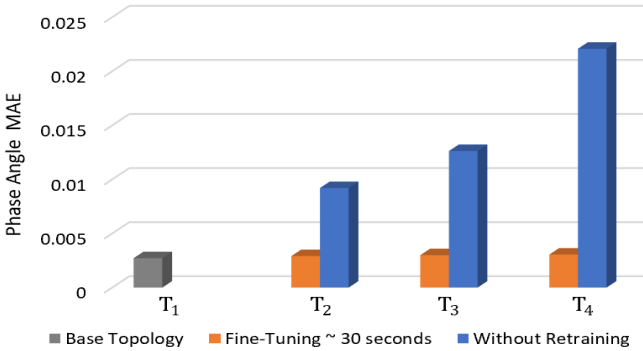


Figure 5: Efficacy of Transfer learning – average Phase angle MAE in rad

C. Impact of Measurement Noise

As noise in measurements is unavoidable, it is important to analyze the impact that different types of noises will have on the performance of a data-driven estimator, such as the DeNSE. It has recently been shown that PMU noises can have non-Gaussian characteristics [14]-[15]. Keeping this in mind, three types of noise characteristics are considered in this study – Gaussian noise, Gaussian mixture model (GMM) noise [16], and Laplacian noise [17]. The Gaussian noise had zero mean, and standard deviation of 0.0033% in magnitude and 0.0029 rad in angle. The GMM noise had two-components having mean, standard deviation, and weight vectors as [0, 0.005]%, [0.0015, 0.0015]%, and [0.3, 0.7], in magnitude, and [0, 0.0043] rad, [0.0014, 0.0014] rad, and [0.3, 0.7], in angle, respectively. The Laplacian noise had a location and scale of 0.001% and 0.0015% in magnitude, and 0.0009 rad and 0.0013 rad, respectively, in angle. The above-mentioned noise parameters corresponded to a TVE of 1% [33]. The results obtained using the DeNSE in presence of these three noise models are shown in Table II. The results obtained using LSE (with 32 locations for PMUs and Gaussian noise) are also provided as a baseline.

From Table II, it becomes clear that the proposed DeNSE gives similar or better performance than LSE for different types of noise models, while requiring *less than half the number of PMUs*. Furthermore, it is also realized that DeNSE is robust enough to handle non-Gaussian measurement noise in an effective manner as there is only a very minor deterioration in performance as the noise models change.

Table II: Performance of DeNSE and LSE under different noise models for 118-bus system

Method	Magnitude MAPE (p.u.)	Angle MAE (rad)	#Buses where PMUs are placed
LSE with Gaussian noise	0.2709	0.0026	32
DeNSE with Gaussian noise	0.1507	0.0027	13
DeNSE with GMM noise	0.1596	0.0029	13
DeNSE with Laplacian noise	0.1543	0.0028	13

D. Impact of Bad Data

To investigate the performance of the proposed nearest OC-based BDDC methodology, we simulate two different scenarios. In the first scenario, we increase the amount of testing samples that are bad, while fixing the severity of the bad data. To do this, the probability of bad data was randomly varied from $\eta = 0\%$ to $\eta = 50\%$ in steps of 10%, while the severity was kept at $\sigma = 3\sigma_0$, where σ_0 denotes the standard deviation of good quality data computed from the training dataset. The results obtained when the proposed methodology is compared with a case where the bad data is not replaced and a case where the bad data is replaced with the mean value from the training dataset (as done in [8]), are shown in Figure 6. It is clear from the figure that in the absence of BDDC, the results become progressively worse as the amount of bad data increases. Moreover, it can be observed that the bad data correction based on the nearest OC consistently outperformed the bad data correction based on mean value for both magnitude and angle estimation as the dotted blue line always lay below the dotted red line (more clearly visible in the inset).

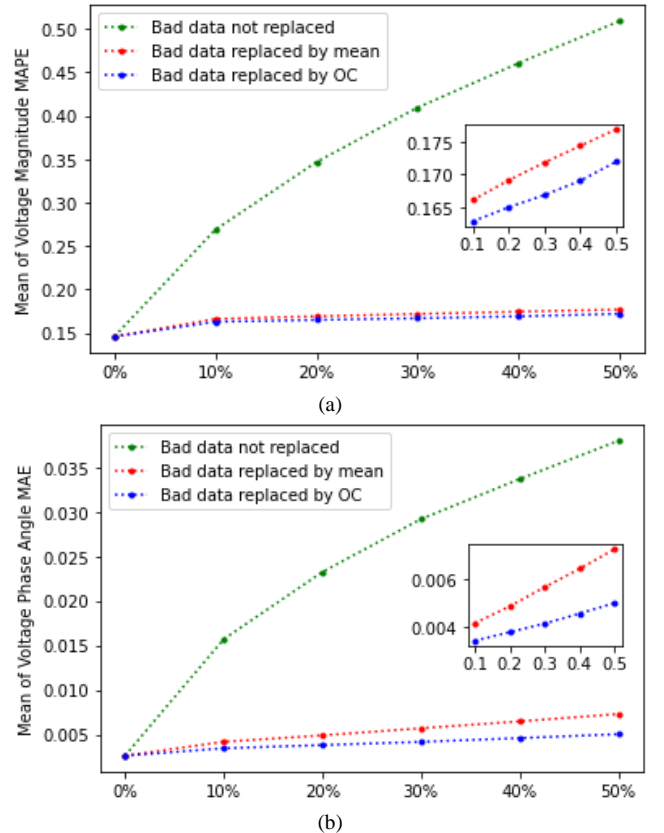


Figure 6: Bad data replacement with increasing probability of bad data

In the second scenario, we increase the severity of the bad data, while fixing the amount of testing samples that are bad. To do this, the severity was increased from $\sigma = 3\sigma_0$ to $\sigma = 7\sigma_0$, while setting $\eta = 30\%$. The results that were obtained when the proposed methodology is compared with the two cases described above (namely, no-replacement and replacement-by-mean), are shown in Figure 7. It is clear from the figure that the proposed methodology for correcting bad data performs much better than the no-replacement case and slightly better than the replacement-by-mean case (as shown in the inset). Lastly, note that the above-mentioned studies were conducted on the trained DNN created in Section IV.A; i.e., only the inputs to the DNN in the testing phase were changed while its architecture was left unaltered.

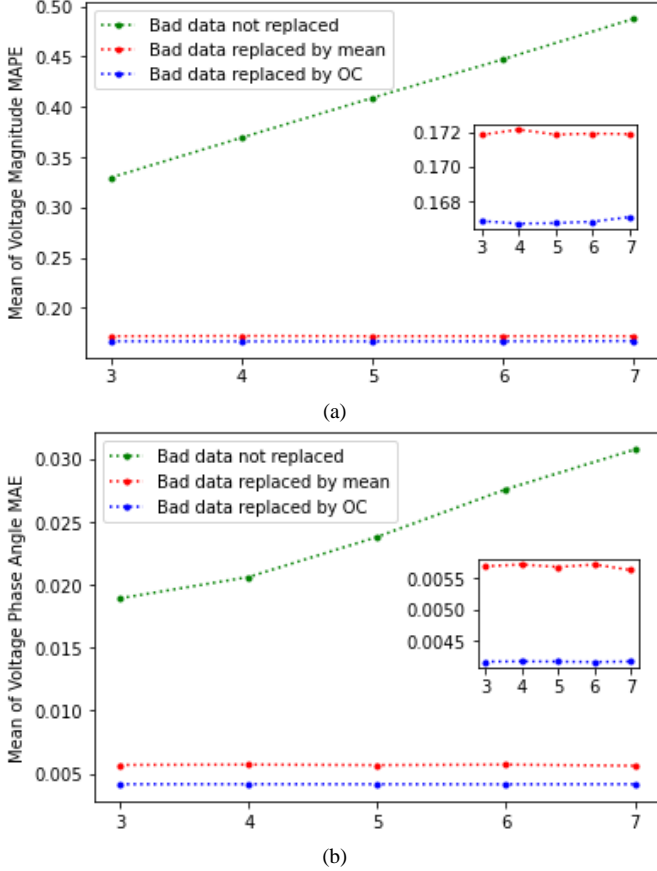


Figure 7: Bad data replacement with increasing severity of bad data

Considering the high-speed at which DeNSE is expected to operate during its online implementation (PMU timescale of 30 samples/second), it must be ensured that the Wald test and data preprocessing is performed within that time-frame. The most time-consuming portion in this regard is the proposed bad data correction module which needs to compare the current testing sample with all the samples in the training database to find the optimal replacement(s). It was observed that with 10,000 training samples and 49 phasor measurements as its inputs, the bad data replacement for the 118-bus system could be carried out in 11.15 ms on average with a standard deviation of 0.92 ms. As this is much less than the speed at which a PMU produces an output (≈ 33 ms), we are confident that the proposed approach will be able to meet the specified high speed and high accuracy expectations of purely PMU-based state estimation.

E. Impact of Extreme Scenarios

In Section IV.D, the superiority of the BDDC methodology based on the Wald test and nearest OC was demonstrated. In this sub-section, the need and impact of extreme scenario filter is discussed. 1,000 extreme scenarios were created in the 118-bus system by significantly increasing the loading of buses 8 and 10. Due to the physics of the power system, PMUs located on these two buses as well as those placed on the buses that are nearby, were impacted in these scenarios. Consequently, one or more measurements coming from these PMUs (i.e., input features of the DeNSE) were flagged as bad data by the Wald test. At the same time, bad data was also added to the PMUs placed on buses 90 and 106, which are far away from the stressed region of the system. The extreme scenario filter identifies the set of features for which the BDDC should be suppressed, using the logic described in Section III.B.2). Three different outcomes were analyzed as shown in Table III. Note that for obtaining the results shown in this table, Gaussian noise was added to all the measurements.

The first row of Table III depicts the outcome that was obtained when the Wald test-based BDDC was absent altogether. The considerable deterioration of the results (compare this row with the second row of Table II) was due to the presence of bad data in the measurements coming from PMUs placed at buses 90 and 106. A large amount of variability was also observed across the 1,000 scenarios as captured by the high standard deviation values of the magnitude MAPE and angle MAE. The second row of Table III depicts the outcome that was obtained when the BDDC took place but the extreme scenario filter was absent. The relatively high errors in this case was due to the presence of extreme scenarios around buses 8 and 10, whose corresponding PMU measurements were unnecessarily replaced. The best outcome was obtained when the Wald test-based BDDC was applied to the PMU measurements coming from buses 90 and 106, but was suppressed by the extreme scenario filter for the PMU measurements coming from the region around buses 8 and 10, as depicted in the third row of Table III. Thus, this analysis demonstrates the robust performance of the proposed DeNSE framework under diverse OCs.

Table III: DeNSE Performance when bad data and extreme scenario manifest simultaneously

Method	Magnitude MAPE (%)		Angle MAE (rad)	
	Mean	Std.	Mean	Std.
DeNSE without BDDC	0.3245	0.0251	0.0173	0.0023
DeNSE with BDDC but without extreme scenario filter	0.2071	0.0038	0.0046	0.0003
DeNSE with BDDC and extreme scenario filter	0.1861	0.0040	0.0034	0.0002

F. State Estimation Results for 2000-Bus Texas System

To demonstrate the applicability of the proposed state estimator to large transmission systems, we use the publicly available 2000-bus Synthetic Texas system [31]. This system has 120 high voltage buses, and it was assumed that PMUs were already placed on these buses such that they were measuring the voltage phasors of these buses as well as the current phasors of the lines that were coming out of these buses. By employing the

time-series data available online for this system [34], the training and testing data was generated and a DNN trained, using the procedure explained in Section III.C.

When the measurements from the PMUs placed on the 120 highest voltage buses of this system were used as inputs to the DNN of the DeNSE, the estimates were found to have a slightly poor accuracy than that obtained using LSE. As such, **Algorithm I** was used to identify new locations where PMUs must be installed; 8 such locations were identified. Table IV shows the error estimates obtained using the DeNSE framework with 128 PMUs and different noise models. Note that LSE for this system requires placing PMUs at 512 optimally selected buses. It can be observed from the table that with PMUs placed in *only one-quarter of the buses* ($128/512 = 0.25$), the proposed approach is able to perform better state estimation than LSE even in presence of non-Gaussian noise in the PMU measurements. The hyperparameters obtained for the DeNSE for this system are summarized in Table V. The tuning of the hyperparameters was done using WandB [32]. Note that the trained DNN took only 2.6 ms on average to produce the state estimates for this system. This validates its ability to estimate the static states of large systems at high speeds.

Table IV: Performance of DeNSE and LSE under different noise models for 2000-bus Texas system

Method	Magnitude MAPE (p.u.)	Angle MAE (rad)	#Buses where PMUs are placed
LSE with Gaussian noise	0.2809	0.0026	512
DeNSE with Gaussian noise	0.2601	0.0022	128
DeNSE with GMM noise	0.2614	0.0023	128
DeNSE with Laplacian noise	0.2636	0.0023	128

Table V: Hyperparameters for DeNSE for 2000-bus Texas system

Hyperparameter	Value
Number of Hidden Layers	4
Number of Neurons per Hidden Layer	500
Activation Functions	ReLU (Hidden Layers) Linear (Output Layer)
Loss Function	Mean Squared Error
Optimizer	ADAM
Batch Size	256
Learning Rate	0.001
Number of Epochs	3,000
Early Stopping	Patience = 10
Dropout	
Dataset size	
Training	7,500
Validation	2,500
Testing	4,000
Total	14,000

V. CONCLUSION

In this paper, a Bayesian framework for high-speed TSSE is proposed that does not require complete observability of the system by PMUs for its successful execution. Machine learning is employed in the proposed state estimator, called DeNSE, to indirectly combine inferences drawn from slow timescale SCADA data with fast timescale PMU measurements. A novel, data-driven PMU placement methodology is also introduced to improve estimation performance. The proposed approach

successfully tackles topology changes, non-Gaussian measurement noise, and different types of bad data under diverse operating conditions.

The IEEE 118-bus system and the 2000-bus Synthetic Texas system were used as the test systems for the analysis conducted here. In comparison to conventional approaches, the proposed DeNSE was able to bring the estimation errors of all the buses to the desired levels while needing *less than half the number of PMUs* for the 118-bus system and *only one-quarter of the PMUs* for the 2000-bus system. The future scope of this work will involve providing statistical guarantees to the performance of the DeNSE framework.

ACKNOWLEDGEMENTS

We thank the financial assistance provided by all the funding agencies that supported this project. Note that the views expressed herein do not necessarily represent the views of the U.S. Department of Energy or the U.S. Government.

REFERENCES

- [1] M. Göl and A. Abur, "A hybrid state estimator for systems with limited number of PMUs," *IEEE Trans. Power Syst.*, vol. 30, no. 3, pp. 1511-1517, May 2015.
- [2] M. Kabiri and N. Amjady, "A new hybrid state estimation considering different accuracy levels of PMU and SCADA measurements," *IEEE Trans. Instrum. Meas.*, vol. 68, no. 9, pp. 3078-3089, Sep. 2019.
- [3] Z. Jin, P. Wall, Y. Chen, J. Yu, S. Chakrabarti and V. Terzija, "Analysis of hybrid state estimators: accuracy and convergence of estimator formulations," *IEEE Trans. Power Syst.*, vol. 34, no. 4, pp. 2565-2576, Jul. 2019.
- [4] T. Chen, H. Ren, Y. Sun, M. Kraft and G. A. J. Amaratunga, "Optimal placement of phasor measurement unit in smart grids considering multiple constraints," accepted for publication in *J. Modern Power Syst. Clean Energy*.
- [5] V. Chakati, M. Pore, A. Pal, A. Banerjee, and S. K. S. Gupta, "Challenges and trade-offs of a cloud hosted phasor measurement unit-based linear state estimator," in *Proc. IEEE Power Eng. Soc. Conf. Innovative Smart Grid Technol.*, Washington DC, pp. 1-5, 23-26 Apr. 2017.
- [6] C. Xu and A. Abur, "Robust linear state estimation using multi-level power system models with different partitions," in *Proc. IEEE PowerTech*, Manchester, UK, pp. 1-5, 18-22 Jun. 2017.
- [7] P. Chatterjee, A. Pal, J. S. Thorp, and J. De La Ree, "Partitioned linear state estimation," in *Proc. IEEE Power Eng. Soc. Conf. Innovative Smart Grid Technol.*, Washington D.C, pp. 1-5, 18-20 Feb. 2015.
- [8] K. R. Mestav, J. Luengo-Rozas, and L. Tong, "Bayesian state estimation for unobservable distribution systems via deep learning," *IEEE Trans. Power Syst.*, vol. 34, no. 6, pp. 4910-4920, Nov. 2019.
- [9] B. Azimian, R. S. Biswas, S. Moshtagh, A. Pal, L. Tong, and G. Dasarathy, "State and topology estimation for unobservable distribution systems using deep neural networks," *IEEE Trans. Instrum. Meas.*, vol. 71, pp. 1-14, Apr. 2022.
- [10] K. R. Mestav and L. Tong, "Learning the unobservable: high-resolution state estimation via deep learning," in *Proc. 57th Annual Allerton Conf. Commun., Control, and Computing*, Monticello, IL, pp. 171-176, 24-27 Sep. 2019.
- [11] G. Tian, Y. Gu, D. Shi, J. Fu, Z. Yu, and Q. Zhou, "Neural-network-based power system state estimation with extended observability," *J. Modern Power Syst. Clean Energy*, vol. 9, no. 5, pp. 1043-1053, Jun. 2021.
- [12] R. Raz, "On the complexity of matrix product," in *Proc. 34th Annu. ACM Symp. Theory Computing*, pp. 144-151, 19 May 2002.
- [13] E. Klarreich, "Multiplication hits the speed limit," *Commun. ACM*, vol. 63, no. 1, pp. 11-13, Jan. 2020.
- [14] T. Ahmad and N. Senroy, "Statistical characterization of PMU error for robust WAMS based analytics," *IEEE Trans. Power Syst.*, vol. 35, no. 2, pp. 920-928, Mar. 2020.
- [15] D. Salls, J. Ramirez, A. Varghese, J. Patterson, and A. Pal, "Statistical characterization of random errors present in synchrophasor measurements," in *Proc. IEEE Power Eng. Soc. General Meeting*, Washington DC, pp. 1-5, 26-29 Jul. 2021.

- [16] A. C. Varghese, A. Pal, and G. Dasarathy, "Transmission line parameter estimation under non-Gaussian measurement noise," accepted for publication in *IEEE Trans. Power Syst.*
- [17] J. Zhao and L. Mili, "A framework for robust hybrid state estimation with unknown measurement noise statistics," *IEEE Trans. Industrial Informatics*, vol. 14, no. 5, pp. 1866-1875, May 2018.
- [18] Y. Gu, Z. Yu, R. Diao and D. Shi, "Doubly-fed deep learning method for bad data identification in linear state estimation," *J. Modern Power Syst. Clean Energy*, vol. 8, no. 6, pp. 1140-1150, Nov. 2020.
- [19] W. Liu, J. Liu, H. Li, Q. Du and Y. -L. Wang, "Multichannel signal detection based on Wald test in subspace interference and Gaussian noise," *IEEE Trans. Aerospace Electron. Syst.*, vol. 55, no. 3, pp. 1370-1381, Jun. 2019.
- [20] Y. Wei, Y. Zhang, J. Huang, and Q. Yang, "Transfer learning via learning to transfer," in *Proc. 35th Int. Conf. Mach. Learning*, Stockholm Sweden, pp. 5085-5094, 10-15 Jul. 2018.
- [21] A. Pal, A. K. S. Vullikanti and S. S. Ravi, "A PMU placement scheme considering realistic costs and modern trends in relaying," *IEEE Trans. Power Syst.*, vol. 32, no. 1, pp. 552-561, Jan. 2017.
- [22] A. Pal, C. Mishra, A. K. S. Vullikanti, and S. S. Ravi, "General optimal substation coverage algorithm for phasor measurement unit placement in practical systems," *IET Gener., Transm. Distrib.*, vol. 11, no. 2, pp. 347-353, Jan. 2017.
- [23] S. Sonoda, and N. Murata, "Neural network with unbounded activation functions is universal approximator," *Appl. Comput. Harmon. Anal.*, vol. 43, no. 2, pp. 233-268, Sep. 2017.
- [24] J. A. D. Massignan, J. B. A. London and V. Miranda, "Tracking power system state evolution with maximum-correntropy-based extended Kalman filter," *J. Modern Power Syst. Clean Energy*, vol. 8, no. 4, pp. 616-626, Jul. 2020.
- [25] A. Pal, G. A. Sanchez-Ayala, V. A. Centeno and J. S. Thorp, "A PMU placement scheme ensuring real-time monitoring of critical buses of the network," *IEEE Trans. Power Del.*, vol. 29, no. 2, pp. 510-517, Apr. 2014.
- [26] S. J. Pan, and Q. Yang, "A survey on transfer learning," *IEEE Trans. Knowledge Data Eng.*, vol. 22, no. 10, pp. 1345-1359, Oct. 2010.
- [27] S. Niu, Y. Liu, J. Wang, and H. Song, "A decade survey of transfer learning (2010-2020)," *IEEE Trans. Artificial Intell.*, vol. 1, no. 2, pp. 151-166, Oct. 2020.
- [28] Y. Zhang, Y. Zhang, and Q. Yang, "Parameter transfer unit for deep neural networks," *Advances Knowledge Discovery Data Mining*, Cham: Springer International Publishing, pp. 82-95, Mar. 2019.
- [29] K. D. Jones, A. Pal, and J. S. Thorp, "Methodology for performing synchrophasor data conditioning and validation," *IEEE Trans. Power Syst.*, vol. 30, no. 3, pp. 1121-1130, May 2015.
- [30] L. Wasserman, "All of statistics: a concise course in statistical inference," *A Concise Course in Statistical Inference*, New York: Springer, vol. 26, pp. 1-442, 2004.
- [31] A. B. Birchfield, T. Xu, K. Shetye, and T. Overbye, "Building synthetic power transmission networks of many voltage levels, spanning multiple areas," in *Proc. 51st Hawaii Int. Conf. Syst. Sci.*, Hilton Waikoloa Village, Hawaii, pp. 2766-2774, 3-6. Jan 2018.
- [32] "Weights & Biases", Accessed on Nov. 22, 2022. [Online]. Available: <https://wandb.ai/site>
- [33] "IEEE/IEC International Standard - Measuring relays and protection equipment - Part 118-1: Synchrophasor for power systems - Measurements," *IEC/IEEE 60255-118-1:2018*, pp.1-78, Dec. 2018.
- [34] H. Li, J. H. Yeo, A. L. Bornsheuer and T. J. Overbye, "The creation and validation of load time series for synthetic electric power systems," *IEEE Trans. Power Syst.*, vol. 36, no. 2, pp. 961-969, Mar. 2021.